10

Natural Phenomenae-I: Static Modelling

Implicit modelling as an underlying metaphor provides a large number of techniques that facilitate building of complex models. The *BlobTree* provides tools that make use of blending, CSG, deformation, precise contact modelling and other procedural techniques. Figure 10.1 shows a sea anemone model that was built using the *BlobTree*. The spines were placed procedurally using spiral phyllotaxis and blended to the base. The base of the anemone deforms to fit the rock using precise contact modelling. In the following sections we explore methods for describing complex models from the natural world using the implicit methodology.

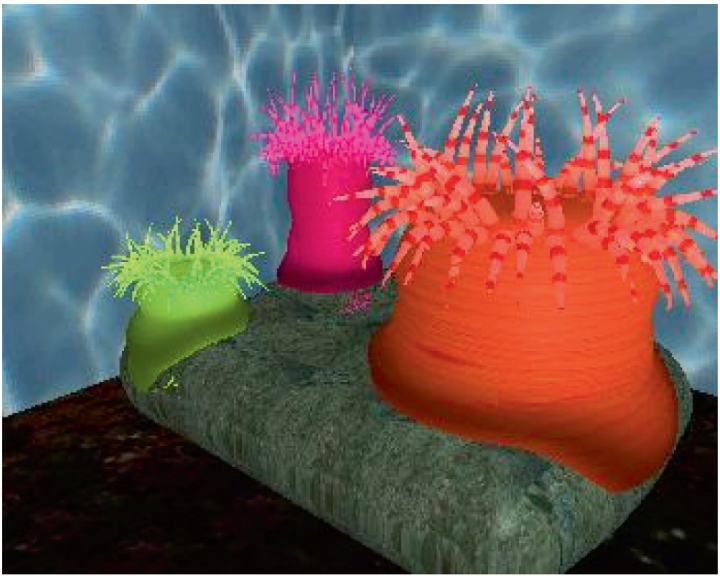

Fig. 10.1. Anemone illustrates the use of PCM to "fit" the rock.

A.J.P. Gomes et al. (eds.), *Implicit Curves and Surfaces: Mathematics, Data Structures and Algorithms*,

10.1 *Murex Cabritii* Shell

The seemingly simple mathematical character of shells, which yield a great variety of beautiful shapes, has attracted much attention from computer modellers. Two motivations for such work are to synthesise realistic images that can be incorporated into computer-generated scenes, and to gain a better understanding of the mechanism of shell formation [144, 266]. Two open problems in the modelling of shells are finding a good method to represent thin spines, and to capture the thickness of the shell walls [144]. In this chapter both of the above problems are addressed using the *BlobTree*. A model of *Murex cabritii* is described which includes large spines, shell walls of non-zero thickness, and allows different textures to be applied to different parts of the shell, while blending textures automatically where these parts join. A preliminary version of this work was published in [152].

10.2 Shell Geometry

As reviewed in [144, 266], the surface of a shell without protrusions may be defined by sweeping a closed generating curve C in the shape of the aperture of the shell along a logarithmic helico-spiral S. The scale of the generating curve increases in geometric progression as the angle of rotation around the shell's axis increases arithmetically.

The helico-spiral is conveniently described in a cylindrical coordinate system (Figure 10.2). The radius R (distance of a point P on the helico-spiral

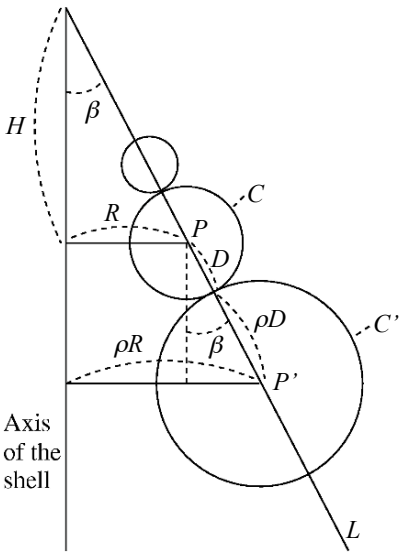

Fig. 10.2. One-half of a longitudinal cross-section of a turbinate shell.

from the shell axis) is an exponential function of the angle of revolution θ around the axis:

$$R(\theta) = R_0 \rho^{(\frac{\theta}{360^\circ})};\ R_0 > 0,\ \rho > 1,\ \theta \geq 0 \tag{10.1}$$

where R_0 is the initial radius and ρ is the ratio of the radii corresponding to a rotation of 360°. The vertical displacement H of point P increases in proportion to the radius:

$$H(\theta) = R(\theta) \cot \beta,\ \beta > 0 \tag{10.2}$$

where β is the angle between the axis of the spiral and a line L passing through successive whorls of the helico-spiral (Figure 10.2). A whorl is defined as a single volution of a spiral shell, or one turn about the axis.

The size of the generating curve C at point P can be determined under the assumption that C is a circle of radius D lying in the plane including the shell axis and the point P, and that the circles in consecutive whorls are tangential to each other. From Figure 10.2 we then obtain:

$$D(\theta) = \frac{R(\theta)}{\sin \beta} \left(\frac{\rho - 1}{\rho + 1} \right) \tag{10.3}$$

In the case of noncircular generating curves, Equation (10.3) remains useful as an approximate indicator of the curve size.

10.3 *Murex Cabritii*

To model *Murex cabritii* requires a description of the parts of the shell. The model is derived from observations made from Figure 10.3, and from a written description of the shell found in [336] page 507, which lists the following features:

Fig. 10.3. *Murex cabritii.*

- A smallish, oval aperture in a strongly convex body whorl.
- A long slender canal below the main body whorl, narrowly open, with three axial rows of four to five spines.
- Each whorl has three varices (ridges) which bear several sharp curving spines.
- Beaded axial riblets (or small bumps) are present between varices.

For the remainder of this chapter a whorl is redefined as a volution of the shell beginning at one varix, and ending after three varices have been formed. From Figure 10.3 it has been estimated that a whorl corresponds to a rotation of $\theta_{\text{whorl}} = 348°$ about the axis of the shell, thus the angle between successive varices θ_{varix} is equal to 116°. This redefinition is employed as model construction is more usefully guided by angles at which varices occur than arbitrary intervals of 360°.

The model presented in this chapter is constructed with $w_{\text{count}} = 7$ whorls, each having $v_{\text{count}} = 3$ varices, thus a total of $w_{\text{count}} v_{\text{count}} = 21$ varices are in the final model. Five to six spines (as observed in Figure 10.3) are modelled in the axial rows rather than four to five as described above. The bumps occur periodically both parallel and perpendicular to the helico-spiral, and five sets of bumps are added along the helico-spiral between each pair of varices. The y-axis in the standard coordinate system is defined as the axis of rotation of the shell. The following parameters are used to define the helico-spiral for the model:

$$\begin{aligned} \beta &= 22.5° \\ \rho &= 1.3 \\ R_0 &= 0.2 \\ D(\theta) &= \tfrac{R(\theta)}{\sin\beta}\tfrac{\rho-1}{\rho+1} = 0.341R(\theta) \end{aligned} \tag{10.4}$$

10.4 Modelling *Murex Cabritii*

Procedural techniques are used to construct a *BlobTree* defining the model of *Murex cabritii*. To implement the procedures introduced in this chapter, the Python interface similar to that outlined in [388] was used. To describe the construction of the *BlobTree*, the following notation is introduced. Arbitrary *BlobTree* models are described using the symbol B, with specific instances denoted using appropriate subscripts. For example, skeletal implicit primitives, which are the basic building blocks from which models are constructed, are denoted as follows:

$$\begin{aligned} B_{\text{point}} &\rightarrow \text{Skeletal point primitive} \\ B_{\text{line}} &\rightarrow \text{Skeletal line primitive} \end{aligned} \tag{10.5}$$

Models are defined by expressions which combine *BlobTrees* using a mixture of basic operators $\cup$ (union), $\cap$ (intersection), $-$ (difference), $+$ (blend),

$\oplus_n$ (super-elliptic blend) and functional composition operators f_{control} (controlled blend), f_{transl} (translate), f_{scale} (scale), f_{rot} (rotate), f_{twist} (twist warp), f_{taper} (taper warp), f_{bend} (bend warp), f_{textG} (gradient interpolated 2D texture mapping), and f_{textF} (field interpolated 2D texture mapping). Additionally $\sum$ and $\bigoplus_n$ are used to represent the blend and super-elliptic blend, respectively, of multiple *BlobTrees* using limit style notation. These operators all correspond to the well-defined implicit surface modelling operations introduced in Chapter 9.

At the lowest level, these operators act on one or more primitives. As a valid *BlobTree* results from each operation, which may be passed as input to other operators, hierarchical models are easily constructed.

The functional composition operators differ from the basic operators in that they require additional parameters to the input *BlobTrees*. Notationally this is defined as $f_{\text{operator}}(p_1, p_2, \ldots, p_n)(B_1, B_2, \ldots, B_m)$ for an arbitrary operator with n parameters and m input *BlobTrees* as follows:

$f_{\text{transl}}(x, y, z)(B)$	$\rightarrow$ translate by (x, y, z)
$f_{\text{scale}}(x, y, z)(B)$	$\rightarrow$ scale by (x, y, z)
$f_{\text{rot}}(\theta, axis)(B)$	$\rightarrow$ rotate by θ about the given axis using the right-hand rule
$f_{\text{transf}}(m)(B)$	$\rightarrow$ transform by matrix m
$f_{\text{taper}}(n)(B)$	$\rightarrow$ taper by n along the positive y-axis
$f_{\text{bend}}(\theta, d)(B)$	$\rightarrow$ bend by θ degrees about the z-axis over a distance of d units
$f_{\text{control}}(b_1, ..., b_n)(B_1, ..., B_m)$	$\rightarrow$ Controlled blend of m *BlobTrees* where each b_i defines a blend group and $b_i \subseteq \{1, ..., m\}$
$f_{\text{textG}}(t)(B)$	$\rightarrow$ apply texture t using gradient interpolated texture mapping
$f_{\text{textF}}(t)(B)$	$\rightarrow$ apply texture t using field interpolated texture mapping

For clarity, the numerical parameters to the above functional composition operators will at times be omitted in the following discussion.

Construction of the *BlobTree* defining a *Murex cabritii* shell is discussed next. Section 10.4.1 describes building the main body whorl of the shell. Creation of the varices is discussed in Section 10.4.2, followed by the addition of bumps in Section 10.4.3 and the spines on the lower canal in Section 10.4.4. Creating the aperture is described in Section 10.4.5 and the application of 2D textures is discussed in Section 10.5.

10.4.1 Main Body Whorl

The formulas in Section 10.2 determine position (Equations (10.1) and (10.2)) and size (Equation (10.3)) of a generating curve along a helico-spiral, such

that if successive curves are placed along the helico-spiral and connected in a polygonal mesh, an approximation of the surface of the shell is obtained. For example, Fowler et al. [144] used piecewise Bézier curves to construct generating curves, which were applied to model a great variety of shells.

A similar method is used to create the implicit model. A generating implicit surface B_g is first defined (for example using a skeletal implicit point primitive). The placement of an instance of B_g on the helico-spiral at any angle θ is then performed in three steps:

1. Scale by $D(\theta)$—Equation (10.3).
2. Translate by $\big(R(\theta),H(\theta),0\big)$—Equations (10.1) and (10.2).
3. Rotate by θ about the y-axis.

that is, the function

$$P(B,\theta) = f_{\text{rot}}\big(\theta, a_y\big) \,.\, f_{\text{transl}}\big(R(\theta), H(\theta), 0\big) \,.\, f_{\text{scale}}\big(D(\theta), D(\theta), D(\theta)\big) \,.\, B \tag{10.6}$$

transforms an arbitrary *BlobTree* B as described above. To construct the whorl, instances of B_g are placed at fixed intervals of θ_g along the helico-spiral using Equation (10.6). The value assigned to θ_g must be chosen with care. If θ_g is too large, then a smooth blend along the helico-spiral will not be realised. In contrast, if θ_g is too small, then the tight overlap of the many instances of B_g will lead to poor blending properties when adding detail to the shell.

To incorporate controlled blending, each whorl is modelled in three whorl sections, which are contained between successive varices along the whorl, and thus correspond to a rotation of θ_{varix} about the axis of the shell. Each whorl section is created by placing five instances of B_g on the helico-spiral such that $\theta_g = \theta_{\text{varix}}/5$. The *BlobTree* for a whorl section ${B_{\text{whorl}}}_v^w$ which immediately precedes varix v on whorl w is given by:

$${B_{\text{whorl}}}_v^w = \sum_{i=1}^{5} P\big(B_g, (3w+v-1)\theta_{\text{varix}} + \theta_g i\big) \tag{10.7}$$

Figure 10.4 shows a whorl section composed of five point primitives placed along a helico-spiral, as the radius of the field defined by each primitive is increased, the resulting blended surface tends toward a shell whorl with a circular aperture.

To avoid unwanted blending between consecutive whorls, controlled blending (see Section 9.5.1) is applied to create the main shell body B_{body} using the following procedure:

$$\begin{aligned} L_{\text{whorlsections}} &= ({B_{\text{whorl}}}_i^j), \text{with } i = 1,\ldots,v_{\text{count}}, j = 1,\ldots,w_{\text{count}} \\ L_{\text{blendpairs}} &= \big\{(j, j+1) : j \in \{1,2,...,w_{\text{count}}v_{\text{count}} - 1\}\big\} \\ B_{\text{body}} &= f_{\text{control}}\big(L_{\text{blendpairs}}\big)\big(L_{\text{whorlsections}}\big) \end{aligned} \tag{10.8}$$

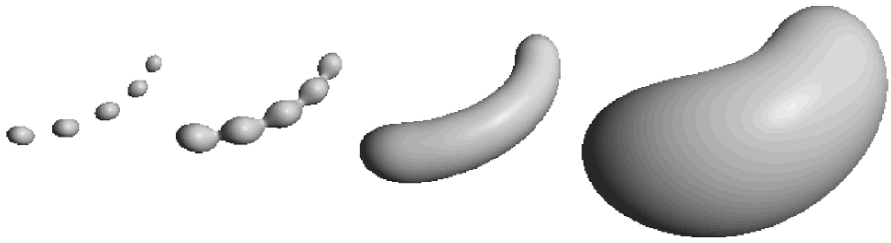

Fig. 10.4. Five point primitives placed on a helico-spiral. As the size of the field produced by each primitive increases, the resulting surface forms part of the main body whorl of a shell.

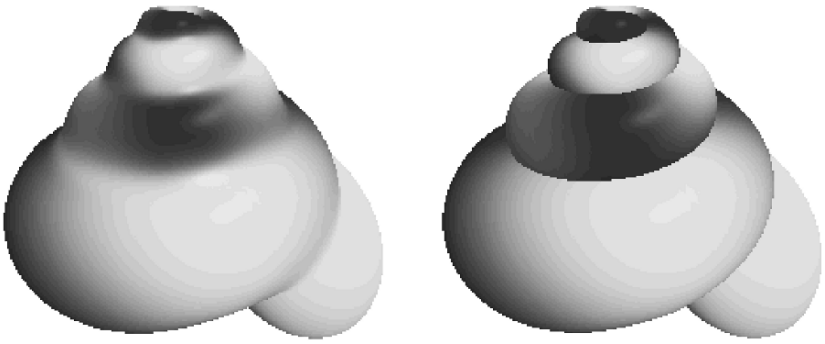

Fig. 10.5. Each whorl of a shell is composed of three sections (shown in Figure 10.4). On the left all sections blend with all other sections, on the right controlled blending constrains each section to blend only with its two neighbours along the helico-spiral.

Each whorl section is blended with its two immediate neighbours, and not with any other whorl sections. The resulting surface is thus smooth along the helico-spiral, while adjacent whorls do not blend together. A comparison of the results obtained with and without controlled blending is shown in Figure 10.5, where four whorls and a total of twelve whorl sections were modelled using a point primitive as the generating surface. The whorl sections are assigned dark and light colours in an alternating pattern so that each whorl section is easily distinguished.

To incorporate the long slender canal below the main body whorl, a tapered line primitive, subsequently bent with a bend operator, was placed below and blended to a point primitive as follows:

$$B_g = f_{\text{transf}}(B_{\text{point}}) + f_{\text{transf}}\Big(f_{\text{bend}}\big(f_{\text{taper}}\big(f_{\text{transf}}(B_{\text{line}})\big)\big)\Big) \tag{10.9}$$

The generating surface and the resulting whorl it defines are shown in Figure 10.6.

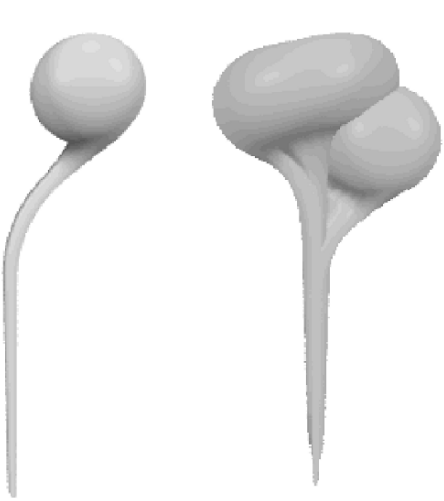

Fig. 10.6. On the left is the generating surface used for the model of *murex cabritii*, on the right is the whorl this surface defines.

10.4.2 Constructing Varices

Varices are the spiny ridges extending out from the main body whorl at even intervals of θ_{varix} around the axis of the shell. The varix is modelled primarily as a series of curving spines of varying size. The relative size and location of spines for varix v on whorl w is determined on a per-whorl basis, (for values see [153]). Individual spines are modelled using tapered line primitives which are bent by 30° over four units of length. Thus, spines shorter than 4 units are bent less than 30°, and spines longer than 4 units are not bent over their whole length. All spines are modelled with the same thickness. By applying taper such that the amount of taper is inversely proportional to the length of each individual spine, a uniform thickness at the tip is achieved, regardless of individual spine length. Construction of the ith spine ${B_{\text{spine}}}_i^w$ for a varix on whorl w using this method.

The left hand image in Figure 10.7 shows the resulting series of spines for $w = 7$ blended to a whorl section. The result does not accurately reflect the form observed in Figure 10.3, as the spines in the varix of *Murex cabritii* are not free-standing, but are blended together in a ridge. A circle primitive (which defined a toroid implicit surface) is added to connect the spines to each other near the shell surface. The effect of this operation is seen in the centre image of Figure 10.7. A new problem now emerges in that the base of the spines are obscured by the toroid ridge. To make the spines stand out from the ridge, a suitable scale is introduced:

$$\begin{aligned} {B_{\text{spine}}}_i^w = {} & f_{\text{bend}}(30,4) \,.\, f_{\text{rot}}(-90,a_z) \,.\, f_{\text{taperZ}}\left(\tfrac{8}{\delta_i^w}\right) \,. \\ & \cdot \; f_{\text{taperX}}\left(\tfrac{4}{\delta_i^w}\right) \,.\, f_{\text{scale}}(1,\delta_i^w,3) \,.\, B_{\text{line}} \end{aligned} \tag{10.10}$$

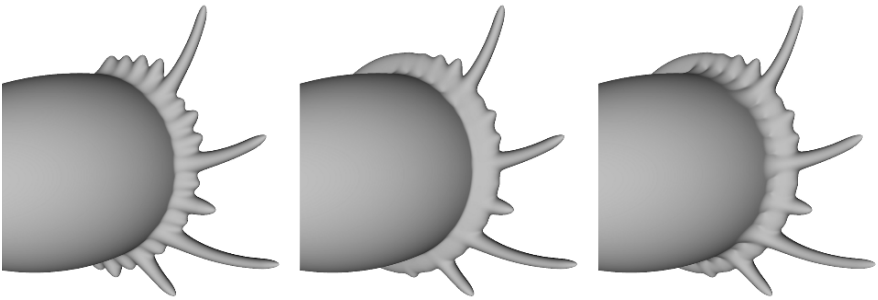

Fig. 10.7. Creation of a varix. Left: bent tapered line primitives are placed as curved spines. Centre: a circle primitive is used to create a toroid ridge blending the spines together. Right: spines are modified as and super-elliptic blending is employed.

where a_z stands for the z-axis and δ_i^w the relative size of curving spines at each of 3 varices per whorl in the model of *murex cabritii*. In this case, the spines are scaled by a factor of 3 in the z axis, and subsequently tapered by an increased amount in the z-axis. The resulting spines are much wider in the z-axis at their base, but gradually revert toward a circular aperture along their length. When the spines are positioned along the helico-spiral, the z-axis in their local coordinate system is transformed to be parallel to the helico-spiral, thus the base of the spines are lengthened along the helico-spiral. Finally, to avoid an overly smooth blending of the spines both with each other, and with the toroid ridge, super-elliptic blending (Equation (9.14)) was used with a blend factor of 3 to blend all of the components of the varix together. The base *BlobTree* for a varix ${B_{\text{varix}}}^w$ on whorl w is thus defined as:

$$ {B_{\text{varix}}}^w = f_{\text{transf}}(B_{\text{circle}}) \oplus_3 \bigoplus_{i=1}^{s_{\text{count}}}{}_3 f_{\text{rot}}\big(\alpha_i, a_z\big)\big(f_{\text{transl}}(r_a, 0, 0)({B_{\text{spine}}}_i^w)\big) \tag{10.11} $$

using ${B_{\text{spine}}}_i^w$ from Equation (10.10). The vth varix ${B_{\text{varix}}}_v^w$ on whorl w is defined by using Equation (10.6) with ${B_{\text{varix}}}^w$ as follows:

$$ {B_{\text{varix}}}_v^w = P\big({B_{\text{varix}}}^w, (3w + v)\theta_{\text{varix}}\big) \tag{10.12} $$

The right image of Figure 10.7 shows the final varix blended with the final whorl section using Equation (10.12), that is the result of ${B_{\text{varix}}}_{v_{\text{count}}}^{w_{\text{count}}} + {B_{\text{whorl}}}_{v_{\text{count}}}^{w_{\text{count}}}$.

10.4.3 Constructing Bumps

Individual bumps B_{bump} were modelled using single point primitives scaled by $(s_x, s_y, s_z) = (1.4, 1.0, 1.5)$ as follows:

$$ B_{\text{bump}} = f_{\text{scale}}(s_x, s_y, s_z)(B_{\text{point}}) \tag{10.13} $$

Five sets of bumps were placed at regular intervals along the helico-spiral between each successive set of varices. Definition of a single set of bumps ${B_{\text{bumpset}}}^{w}$ for whorl w is done in a similar fashion to the placement of spines on a varix, utilising a set of empirically determined values. One bump was placed for every two spines present in the varices for the given whorl as follows:

$$ {B_{\text{bumpset}}}^{w} = \sum_{i=1}^{s_{\text{count}}/2} f_{\text{rot}}\left(\alpha_{2i}, a_z\right)\left(f_{\text{transl}}(r_a, 0, 0)(B_{\text{bump}})\right) \tag{10.14} $$

To place five sets of bumps ${B_{\text{bumpsection}}}_{v}^{w}$ before a given varix v on whorl w, where $(3w+v)\theta_{\text{varix}}$ is the angle of the varix along the helico-spiral, Equation (10.6) is used as follows:

$$ {B_{\text{bumpsection}}}_{v}^{w} = \sum_{i=1}^{5} P\left({B_{\text{bumpset}}}^{w}, \left(3w + v - 1 + \frac{i}{6}\right)\theta_{\text{varix}}\right) \tag{10.15} $$

The left image of Figure 10.8 shows the final bump section and final whorl section blended together using Equation (10.15), that is the result of ${B_{\text{bumpsection}}}_{v_{\text{count}}}^{w_{\text{count}}} + {B_{\text{whorl}}}_{v_{\text{count}}}^{w_{\text{count}}}$. The bumps are placed as desired; however, the overlap in blending regions causes undesirable amounts of blending between adjacent bumps. The first step to solving this problem is to employ super-elliptic blending again. For the *Murex cabritii* model $n = 3$ has been found to work well.

A localised method is used to provide additional relief for the more tightly packed bumps on the top and bottom of the whorl. Bumps are scaled based on their rotation from the horizontal plane again as defined by empirically determined values for α_i. To produce a more organic feel, the sizes of individual bumps were further modified using the function normal(μ, σ), which returns a pseudo-random number with a normal distribution, where μ is the mean and σ is the standard deviation. The default scale values $\left(s_x, s_y, s_z\right)$ are thus replaced by $\left(s'_x, s'_y, s'_z\right)$ defined as follows:

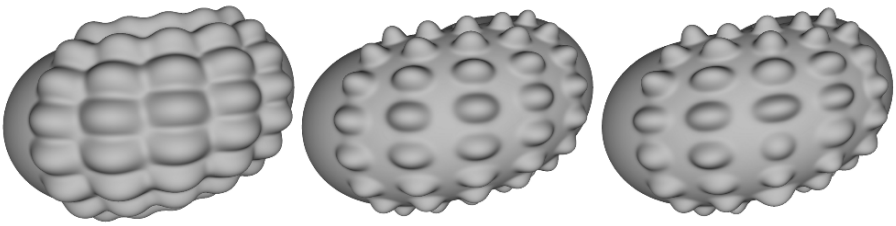

Fig. 10.8. Creation of bumps. Left: bumps arranged and blended. Centre: non-uniform scaling and super-elliptic blending $\oplus_3$ are applied. Right: bumps are randomly scaled, and rotated such that their long axis is aligned locally with the helico-spiral.

$$\begin{aligned} s'_x &= \text{normal}\left(s_x, \tfrac{s_x}{10}\right) \\ s'_y &= \text{normal}\left(s_y, \tfrac{s_x}{10}\right) \\ s'_z &= \text{normal}\left(s_z, \tfrac{s_x}{10}\right) \end{aligned} \tag{10.16}$$

An additional problem arises because the bumps are scaled non-uniformly, so they are not locally aligned with the helico-spiral. This effect can be observed in both the left and centre images from Figure 10.8. To counteract this effect, each individual bump is rotated about the x-axis before they are positioned, such that their longer axis is locally parallel to the helico-spiral.

10.4.4 Constructing Axial Rows of Spines

One row of axial spines protrudes from the lower canal below each varix on the last whorl of the shell. Individual axial spines B_{axspine} are modelled using tapered line primitives, in a similar fashion to the curving spines in the varices from Equation (10.10). The relative sizes and number of axial spines are determined separately for each row. The resulting spines, blended with the lower whorl, are shown in the left image of Figure 10.9.

As with the bumps, to produce a more organic looking object random variation is introduced. Each spine is randomly bent by 3° to 9°, one to three times, using a corresponding number of bend operators. The result is shown in the right image of Figure 10.9. For details of the spine placement, the reader is referred to Galbraith [153].

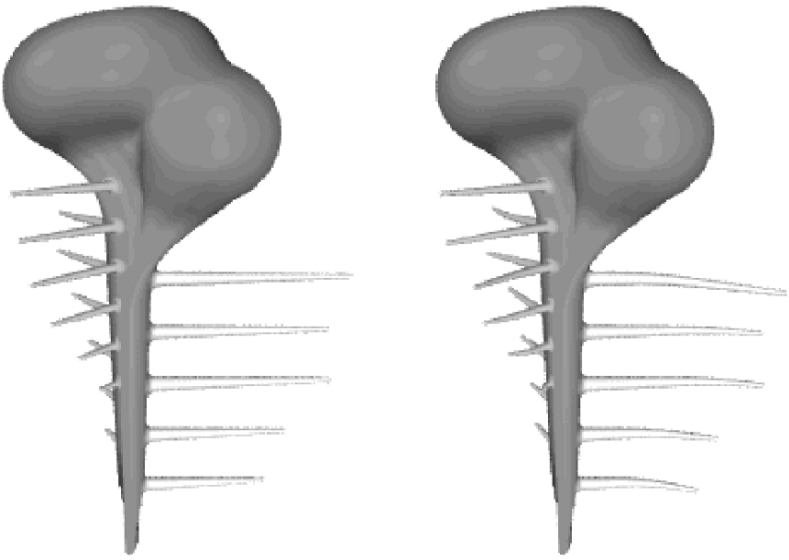

Fig. 10.9. Axial rows of 5-6 spines. Left: spines are straight. Right: each spine is randomly bent 3° to 9° 1-3 times.

10.4.5 Construction of the Aperture

To create the aperture, a solid model, defined as B_{aperture}, is constructed in the shape of the aperture. A CSG difference operation is then used to remove this material from the main body of the shell, thus creating an opening. B_{aperture} is modelled using the same technique as that described for the main body whorl.

A generating surface given by

$$B_{g_{\text{aperture}}} = f_{\text{transf}}(B_{\text{point}}) + f_{\text{transf}}(B_{\text{cone}}) + \\ + f_{\text{transf}}\Big(f_{\text{bend}}\Big(f_{\text{taper}}\big(f_{\text{transf}}(B_{\text{line}})\big)\Big)\Big) \tag{10.17}$$

is created, which is slightly smaller in each dimension orthogonal to the helicospiral, than B_g. Equation (10.17) defines $B_{g_{\text{aperture}}}$, which is formed in a similar fashion to B_g. A point primitive slightly smaller than that of the main whorl's, is blended to a tapered and subsequently bent line primitive, also slightly smaller than that of B_g. To this is also added an inverted cone primitive which extends the inner edge of $B_{g_{\text{aperture}}}$ to the edge of the previous whorl. This is done to ensure that no material is left between the outer shell wall and that of the previous whorl. From Equation (10.17), and similar to Equation (10.7), the corresponding whorl section B_{apwhorl} is defined as follows:

$$B_{\text{apwhorl}} = \sum_{i=1}^{7} P\big(B_{g_{\text{aperture}}}, (w_{\text{count}} v_{\text{count}} - 1)\theta_{\text{varix}} + \theta_g \,.\, i\big) \tag{10.18}$$

Equation (10.18) describes a whorl equivalent to ${B_{\text{whorl}}}_{v_{\text{count}}}^{w_{\text{count}}}$ plus two additional instances of $B_{g_{\text{aperture}}}$. This implies that the aperture will extend θ_{varix} degrees into the shell from the opening. The two additional instances of $B_{g_{\text{aperture}}}$ ensure that B_{apwhorl} extends beyond the termination of ${B_{\text{whorl}}}_{v_{\text{count}}}^{w_{\text{count}}}$, which in turn ensures that the aperture makes a clean opening. $B_{g_{\text{aperture}}}$ and B_{apwhorl} are shown in the left and centre images of Figure 10.10. As defined, B_{apwhorl} is not suitable for creating the opening in the shell, because B_{apwhorl} overlaps significantly with the previous whorl. Before it is used to create the opening, one more modelling operation is performed, shown in the right image of Figure 10.10. A difference operation is used to remove the previous whorl from B_{apwhorl}, thus defining B_{aperture}, which creates an opening in the shell.

$$B_{\text{aperture}} = B_{\text{apwhorl}} - \sum_{v=1}^{v_{\text{count}}} {B_{\text{whorl}}}_{v}^{w_{\text{count}}-1} \tag{10.19}$$

The summation term defines the second to last whorl using Equation (10.7). The right image in Figure 10.10 shows the resulting model. The aperture in the main shell body is then created as:

$$B_{\text{bodywithaperture}} = B_{\text{body}} - B_{\text{aperture}} \tag{10.20}$$

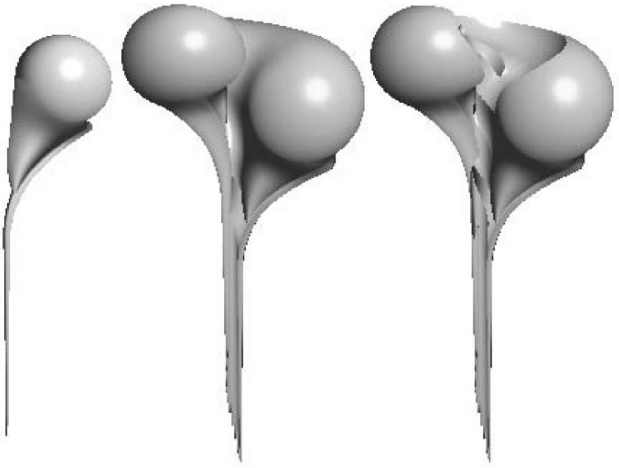

Fig. 10.10. Creating an aperture. Left: the generating surface $B_{g_{\text{aperture}}}$. Centre: the resulting whorl from Equation (10.18). Right: the final aperture after difference is applied to remove the previous whorl.

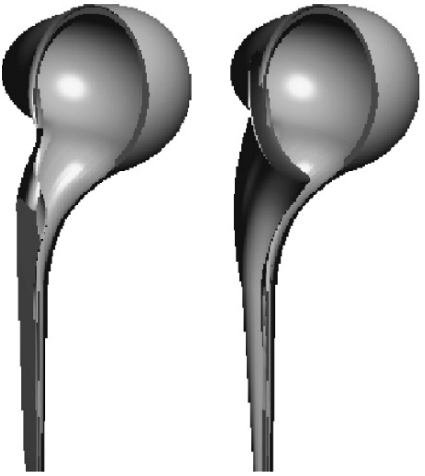

Fig. 10.11. Creating the aperture. Left: the opening which is carved out by Equation (10.20). Right: the final shape of the opening after adding in $B_{\text{insidewall}}$ as in Equation (10.21).

where B_{body} is the complete shell without the opening from Equation (10.9).

The left image in Figure 10.11 shows the result when subtracting B_{aperture} from the last whorl section alone. This figure illustrates that the opening is present only in the last third of the last whorl; however, this is a sufficient size of opening for any view position set outside the shell to give the impression

that the shell is hollow. Only if the view position is set inside the aperture is the solid nature of the model revealed.

A more serious problem arises from the observation that the aperture should be oval (as described in Section 10.3). To generate the desired oval aperture, $B_{\text{bodywithaperture}}$ is revised to include an inside wall:

$$B_{\text{bodywithaperture}} = (B_{\text{body}} - B_{\text{aperture}}) \cup B_{\text{insidewall}} \tag{10.21}$$

$B_{\text{bodywithaperture}}$ with and without the inside wall is shown in Figure 10.11.

10.5 Texturing the Shell

The final step in producing a photorealistic model of *Murex cabritii* is the application of four 2D textures, using two separate texturing methods. The textures used are shown in Figure 10.12, and were created using standard paint programs.

Each whorl section in the main body whorl is textured with the texture shown in Figure 10.12(a) using gradient interpolated texture mapping f_{textG} [387]. This method allows a single texture to be applied to an arbitrary *BlobTree*. As whorl sections are blended to each other, the resulting textures on each whorl section are blended together. By placing the varices directly over these regions, discontinuities in the resulting texture blends are concealed.

Note that since the original work was done on texturing the shell, several new techniques have been designed to ease the task of texturing any point set object. Work is proceeding on this field but the following paper is of interest, [353].

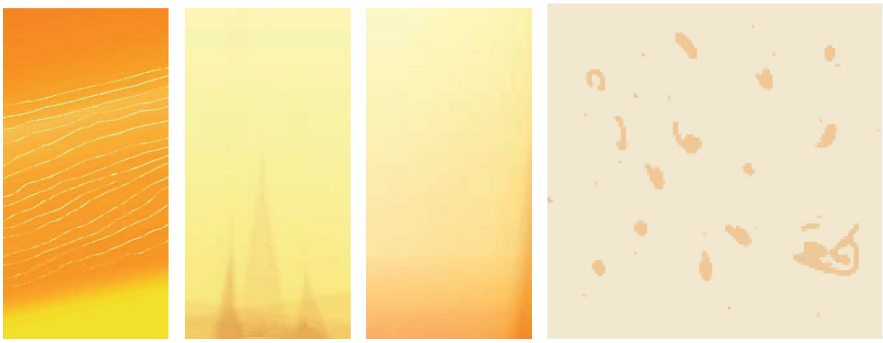

Fig. 10.12. Textures and their corresponding uses in the model of *Murex cabritii*: (a) main body whorl; (b) spines in varices; (c) axial rows of spines; (d) bumps on main whorl.

10.6 Final Model of *Murex Cabritii*

It is now possible to redefine the main geometry of the shell B_{body} (originally defined in Equation (10.9)), including textures, as follows:

$$\begin{aligned} B_{\text{vbwhorl}}{}_v^w &= f_{\text{textG}}(B_{\text{whorl}}{}_v^w) + f_{\text{textF}}(B_{\text{varix}}{}_v^w) + f_{\text{textF}}(B_{\text{bumpsection}}{}_v^w) \\ L_{\text{whorlsections}} &= (B_{\text{whorl}}{}_i^j), \text{with } i = 1, \ldots, v_{\text{count}},\ j = 1, \ldots, w_{\text{count}} \\ L_{\text{blendpairs}} &= \big\{(j, j+1) : j \in \{1, 2, ..., w_{\text{count}} v_{\text{count}} - 1\}\big\} \\ B_{\text{body}} &= f_{\text{control}}\big(L_{\text{blendpairs}}\big)\big(L_{\text{whorlsections}}\big) \end{aligned} \tag{10.22}$$

The key change between Equations (10.9) and 10.22, is the use of $B_{\text{vbwhorl}}{}_v^w$ in place of $B_{\text{whorl}}{}_v^w$. $B_{\text{vbwhorl}}{}_v^w$ incorporates texture maps, and blends a whorl section with its corresponding varix and bump section. Starting with this formulation for B_{body}, the *BlobTree* model of *Murex cabritii* B_{murex} is defined as follows:

$$B_{\text{murex}} = (B_{\text{body}} - B_{\text{aperture}}) \cup B_{\text{insidewall}} + f_{\text{textF}}(B_{\text{axspinerows}}) \tag{10.23}$$

10.7 Shell Results

A comparison of a photograph of *Murex cabritii*, with the resulting model of *Murex cabritii* defined by Equation (10.23), is shown in Figure 10.13. The following areas of the model remain open to improvement: the opening was modelled by observing the opening on similar shells (*Murex troschel*); the position and number of spines and bumps were based on a single view of the shell, the number and placement of these features was arbitrary and suddenly change from one whorl to another; the textures were created in a paint program and pasted on to give a good approximation only; the varices do not extend to the lower canal. A major extension of the model would be to use reaction diffusion techniques [144] to place spines and bumps on the shell.

10.8 Final Remarks

The description of the model of *Murex cabritii* presented in this chapter illustrates how the *BlobTree* may be used to construct models of complex phenomena, based solely on simple geometric primitives and a small set of implicit surface modelling operations. This demonstrates concretely that not only implicit surfaces are a valid choice for modelling natural forms, but in addition that they can create models for which other methods such as L-systems fail. Specifically, large protrusions on a shell surface have been modelled simply by switching from a parametric to an implicit definition of the shell form.

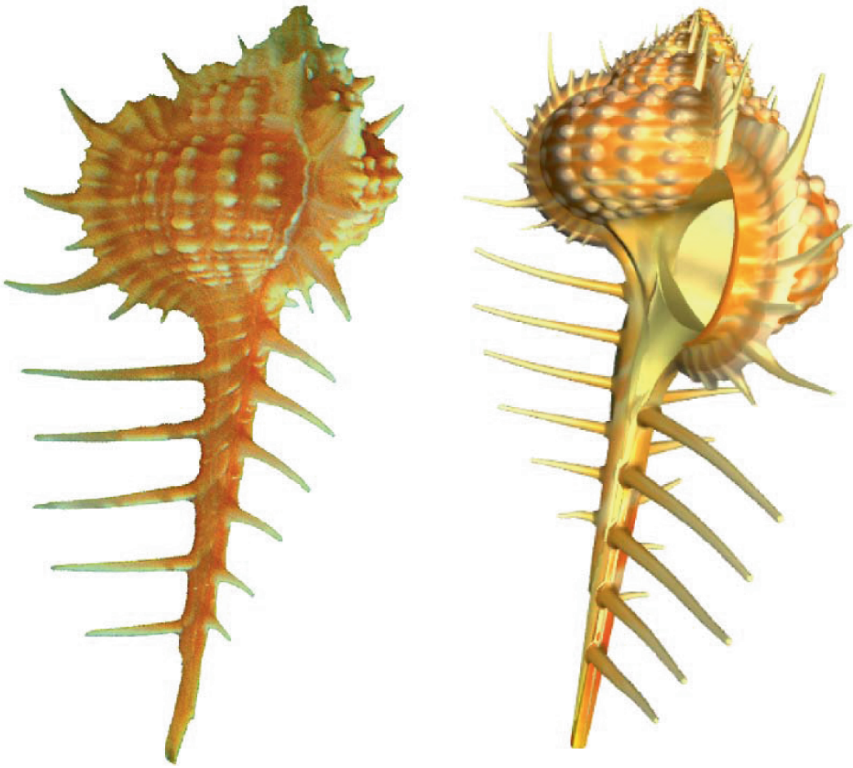

(a) (b)

Fig. 10.13. (a) *Murex cabritii*; (b) model of *Murex cabritii*.